# Overlapping Schwarz Preconditioning for High Order Edge Finite Elements: Application to the Time-Harmonic Maxwell's Equations

Marcella Bonazzoli, Victorita Dolean, Frédéric Hecht, Francesca Rapetti

▶ **To cite this version:**

Marcella Bonazzoli, Victorita Dolean, Frédéric Hecht, Francesca Rapetti. Overlapping Schwarz Preconditioning for High Order Edge Finite Elements: Application to the Time-Harmonic Maxwell's Equations. 2016. hal-01298938v1

**HAL Id: hal-01298938**

**https://hal.science/hal-01298938v1**

Preprint submitted on 6 Apr 2016 (v1), last revised 12 Nov 2017 (v3)

**HAL** is a multi-disciplinary open access archive for the deposit and dissemination of scientific research documents, whether they are published or not. The documents may come from teaching and research institutions in France or abroad, or from public or private research centers.

L'archive ouverte pluridisciplinaire **HAL**, est destinée au dépôt et à la diffusion de documents scientifiques de niveau recherche, publiés ou non, émanant des établissements d'enseignement et de recherche français ou étrangers, des laboratoires publics ou privés.

# OVERLAPPING SCHWARZ PRECONDITIONERS FOR HIGH ORDER EDGE FINITE ELEMENTS: APPLICATION TO THE TIME-HARMONIC MAXWELL'S EQUATIONS*

M. BONAZZOLI†, V. DOLEAN‡, F. HECHT§, AND F. RAPETTI†

**Abstract.** Developing high-speed microwave field measurement systems for wireless, medical or engineering industries is a challenging task. These systems generally rely on high frequency (from 1 to 60GHz) electromagnetic wave propagation in waveguides. High order discretizations of PDEs are well suited for wave propagation since they can provide a highly accurate solution with very low dispersion and dissipation errors. However, the resulting algebraic linear systems can be ill conditioned, so that preconditioning becomes mandatory. In this work, suitable domain decomposition preconditioners for the solution of linear systems resulting from high order edge element discretizations of the time-harmonic Maxwell's equations are described, and validated numerically on 2d and 3d waveguide configurations. The implementation issue of high order edge elements is also discussed in detail.

**Key words.** High order finite elements, edge elements, Schwarz preconditioners, time-harmonic Maxwell's equations.

**AMS subject classifications.** 65N55, 65N35, 65F10

**1. Introduction.** The development of a robust and accurate numerical inversion methodology for microwave imaging is based on three main research areas, often disjoint: optimization, inverse problems and numerical models for the solution of the direct problem modeled by Maxwell's equations. The latter implies the mastery of approximation and solution methods (domain decomposition parallel solvers, parallel computing). The precise simulation of the direct problem in the case of a complex and strongly heterogeneous environment in frequency domain is a challenge in itself. Overall, these features motivate the use of finite element type discretization methods based on high order approximations. After the discretization step, we get very large algebraic systems of equations. To deal with this aspect, parallel computing is mandatory and with it, domain decomposition methods [14].

The earliest domain decomposition method for the time-harmonic Maxwell's equations was proposed by Després in [9]. Further improvements were proposed by Collino [8] using modified, more efficient Robin transmission conditions at the interfaces between subdomains. Over the last decade, a new class of overlapping Schwarz methods was developed for scalar partial differential equations, namely the optimized Schwarz methods. These methods are based on a classical overlapping domain decomposition, but they use more effective transmission conditions than the classical Dirichlet conditions at the interfaces between subdomains [13]. We can distinguish two basic formulations for Maxwell's equations: the first order formulation, for which complete optimized results are known also in the case of conductive medium [17], and the second order (or curl-curl) formulation, with partial optimization results obtained in various

*This work was supported by the French National Research Agency (ANR) in the framework of the project MEDIMAX, ANR-13-MONU-0012.

†Laboratoire J.A. Dieudonné, University of Nice Sophia Antipolis, Parc Valrose, 06108 Nice Cedex 02, France. E-mail: marcella.bonazzoli@unice.fr, francesca.rapetti@unice.fr.

‡Department of Mathematics and Statistics, University of Strathclyde, Glasgow, UK, and Laboratoire J.A. Dieudonné, University of Nice Sophia Antipolis, Nice, France. E-mail: victorita.dolean@strath.ac.uk, victorita.dolean@unice.fr.

§Laboratoire J.L. Lions, Pierre and Marie Curie University, 4 place Jussieu, 75252 Paris Cedex 05, France. E-mail: frederic.hecht@upmc.fr.

works. It has been shown lately that the convergence factors and the optimization process for the two formulations are the same [12]. For the Schwarz algorithms solving the time-harmonic Maxwell's equations promising numerical results have been obtained for standard low order finite volume and finite element methods [15]. All previous methods can be used both as iterative solvers (although not converging for all frequencies present in the error), but more frequently as preconditioners for a Krylov method. As a general rule, it is widely recognized that domain decomposition methods or preconditioners are key in solving efficiently Maxwell's equations in time-harmonic regime.

The development of Schwarz algorithms and preconditioners in the framework of high order finite element methods is still a difficult issue especially in the three-dimensional case. In this work we propose Schwarz preconditioners based on impedance transmission conditions for the high order discretization of the curl-curl formulation of Maxwell's equations. With Maxwell's equations, finite element discretization methods have to be able to represent a field from a finite number of degrees of freedom (dofs) and the nature of dofs (circulations, fluxes, etc.) associates them with geometrical mesh elements other than nodes, such as edges or faces. Indeed, one needs to recognize that different physical quantities have different properties and must be treated accordingly. Whitney finite elements are thus generally adopted [7, 24]. To obtain a more accurate reconstruction of the computed field at a fixed number of unknowns, we need to adopt a high order version of Whitney finite elements, as those recently developed in [29, 30] (for other possible high order finite element bases see for example [1, 31, 23, 21, 2]).

The paper is organized as follows. In Section 2 we introduce the model time-harmonic problem and its variational formulation. In Section 3 we present its high order edge element discretization with particular attention to the implementation of these finite elements. The overlapping Schwarz preconditioners we used are described in Section 4, together with several numerical results about the convergence of the preconditioned iterative method solving the two-dimensional problem. Section 5 closes the presentation with the results in the three-dimensional case.

**2. Physical problem and its weak formulation.** Waveguides are used to transfer electromagnetic power efficiently from one point in space, where an antenna is located, to another, where electronic components treat the in/out information. Rectangular waveguides, which are considered here, are often used to transfer large amounts of microwave power at frequencies greater than 2 GHz. To simulate the electromagnetic wave propagation in such waveguide structures, we work in the frequency domain, thus restricting the analysis to time-harmonic electromagnetic field varying with an angular frequency $\omega > 0$. For all times $t \in \mathbb{R}$, we consider the representation of the electric field $\mathcal{E}$ and the magnetic field $\mathcal{H}$ as

$$\mathcal{E}(\mathbf{x}, t) = \Re(\mathbf{E}(\mathbf{x})e^{\mathtt{i}\omega t}), \qquad \mathcal{H}(\mathbf{x}, t) = \Re(\mathbf{H}(\mathbf{x})e^{\mathtt{i}\omega t}),$$

where $\mathbf{E}(\mathbf{x})$, $\mathbf{H}(\mathbf{x})$ are the complex amplitudes, for all $\mathbf{x} \in \mathcal{D}$, $\mathcal{D} \subset \mathbb{R}^3$ being the considered physical domain. The mathematical model is thus given by the *time-harmonic Maxwell's equations*:

$$\nabla \times \mathbf{H} = \mathtt{i}\omega\varepsilon_\sigma \mathbf{E}, \qquad \nabla \times \mathbf{E} = -\mathtt{i}\omega\mu\mathbf{H}$$

where $\mu$ is the magnetic permeability and $\varepsilon_\sigma$ the electric permittivity of the considered medium in $\mathcal{D}$. To include dissipative effects, we work with a complex valued $\varepsilon_\sigma$, related

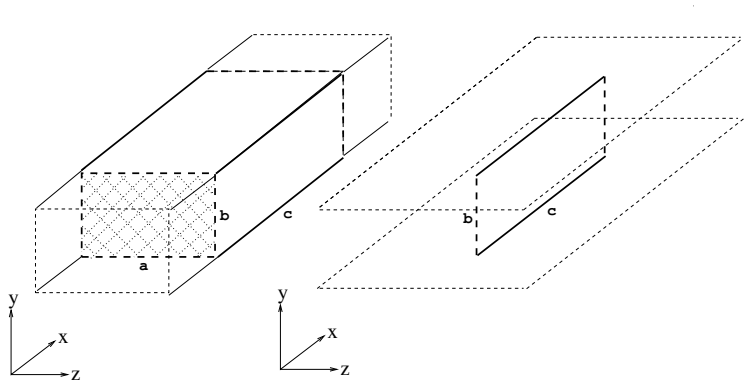


Fig. 2.1: Rectangular waveguide configuration for 3d (left) and 2d (rigth) problems with wave propagation in the $x$-direction. The physical domain $\mathcal{D}$ is in thin line, with dashed style for those boundaries that should be extended to infinity. The computational domain $\Omega$ is in thick line, with dashed style for those boundaries where suitable non reflecting conditions are imposed. These latter are indeed fictitious boundaries of $\Omega$ which are introduced to bound the domain for the numerical simulation of wave propagation in unbounded media.

to the dissipation-free electric permittivity $\varepsilon$ and the electric conductivity $\sigma$ by the relation $\varepsilon_\sigma = \varepsilon - \mathtt{i}\frac{\sigma}{\omega}$. This assumption holds in the regions of $\mathcal{D}$ where the current density $\mathbf{J}$ is of conductive type, that is, $\mathbf{J}$ and $\mathbf{E}$ are related by Ohm's law $\mathbf{J} = \sigma\mathbf{E}$. Both $\varepsilon$ and $\mu$ are supposed to be positive, bounded functions. Expressing Maxwell's equations in terms of the electric field and supposing that $\mu$ is constant, we obtain

$$\nabla \times (\nabla \times \mathbf{E}) - \gamma^2 \mathbf{E} = \mathbf{0}, \tag{2.1}$$

where the (complex) constant $\gamma$ is related to the physical parameters as follows

$$\gamma = \sqrt{\omega^2\mu\varepsilon - \mathtt{i}\omega\mu\sigma} = \omega\sqrt{\mu\varepsilon_\sigma}, \qquad \varepsilon_\sigma = \varepsilon - \mathtt{i}\frac{\sigma}{\omega}.$$

Notice that if $\sigma = 0$, we have $\gamma = \tilde{\omega}$, $\tilde{\omega} = \omega\sqrt{\mu\varepsilon}$ being the wavenumber.

Equation (2.1) is to be solved in a suitable bounded section $\Omega$ of the physical domain $\mathcal{D}$, as shown in Fig. 2.1. In the 3d case, the physical domain $\mathcal{D} \subset \mathbb{R}^3$ is an infinite 'parallelepiped' parallel to the $x$-direction and the computational domain is a bounded section, say $\Omega = (0, \mathtt{X}) \times (0, \mathtt{Y}) \times (0, \mathtt{Z}) = (0, \mathtt{c}) \times (0, \mathtt{b}) \times (0, \mathtt{a})$ of $\mathcal{D}$. In the 2d case, the physical domain $\mathcal{D} \subset \mathbb{R}^3$ is the space contained between two infinite parallel metallic plates, say $y = 0$, $y = \mathtt{b}$, and all physical parameters $\mu$, $\sigma$, $\varepsilon$ have to be supposed invariant in the $z$-direction. The computational domain in 2d is a bounded section, say $\Omega = (0, \mathtt{X}) \times (0, \mathtt{Y}) = (0, \mathtt{c}) \times (0, \mathtt{b})$, of $\mathcal{D}$. In both 2d and 3d cases, the wave propagates in the $x$-direction within the domain.

Let $\mathbf{n}$ be the unit outward normal to $\partial\Omega$. We solve the boundary value problem given by equation (2.1), with metallic boundary conditions

$$\mathbf{E} \times \mathbf{n} = \mathbf{0}, \text{ on } \Gamma_{\mathrm{w}},$$

on the waveguide perfectly conducting walls $\Gamma_{\mathrm{w}} = \{\mathbf{x} \in \partial\Omega,\ \mathbf{n}(\mathbf{x}) \cdot \mathbf{e}_x = 0\}$, with

$\mathbf{e}_x = (1,0,0)^t$, and impedance boundary conditions

$$(\nabla \times \mathbf{E}) \times \mathbf{n} + \mathtt{i}\xi \mathbf{n} \times (\mathbf{E} \times \mathbf{n}) = \mathbf{g}^{\text{in}}, \text{ on } \Gamma_{\text{in}}, \qquad \xi \in \mathbb{R}_{>0},$$
$$(\nabla \times \mathbf{E}) \times \mathbf{n} + \mathtt{i}\xi \mathbf{n} \times (\mathbf{E} \times \mathbf{n}) = \mathbf{g}^{\text{out}}, \text{ on } \Gamma_{\text{out}},$$

at the waveguide entrance $\Gamma_{\text{in}} = \{\mathbf{x} \in \partial\Omega, \ \mathbf{n}(\mathbf{x}) \cdot \mathbf{e}_x < 0\}$, and exit $\Gamma_{\text{out}} = \{\mathbf{x} \in \partial\Omega, \ \mathbf{n}(\mathbf{x}) \cdot \mathbf{e}_x > 0\}$. The vectors $\mathbf{g}^{\text{in}}$, $\mathbf{g}^{\text{out}}$ depend on the incident wave. On one hand, impedance conditions on the artificial boundaries $\Gamma_{\text{in}}$, $\Gamma_{\text{out}}$ are defined to let outgoing waves pass through $\Omega$ unaffected; they mathematically translate the fact that $\Omega$ is a truncated part of an infinite domain $\mathcal{D}$. On the other hand, they simply model the fact that the waveguide is connected to electronic components such as co-axial cables or antennas.

In 2d the function $\mathbf{E}_{\text{ex}} = (0, e^{-\mathtt{i}\gamma x})$ verifies the equation, the metallic boundary conditions on $\Gamma_{\text{w}}$, and the impedance boundary conditions on $\Gamma_{\text{in}}$, $\Gamma_{\text{out}}$ with parameter $\xi = \tilde{\omega}$ and $\mathbf{g}^{\text{in}} = (\mathtt{i}\gamma + \mathtt{i}\tilde{\omega})\mathbf{E}_{\text{ex}}$ and $\mathbf{g}^{\text{out}} = (-\mathtt{i}\gamma + \mathtt{i}\tilde{\omega})\mathbf{E}_{\text{ex}}$; when $\sigma = 0$ we get $\mathbf{g}^{\text{in}} = 2\mathtt{i}\tilde{\omega}\mathbf{E}_{\text{ex}}$ and $\mathbf{g}^{\text{out}} = \mathbf{0}$. The real part of the propagation constant $-\mathtt{i}\gamma$ gives the rate at which the amplitude changes as the wave propagates, thus indications on wave dissipation (notice that if $\sigma > 0$, $\Re(-\mathtt{i}\gamma) < 0$, while if $\sigma = 0$, $\Re(-\mathtt{i}\gamma) = 0$).

In 3d, if $\sigma = 0$ we consider the exact solution given by the Transverse Electric (TE) modes, with $m, n \in \mathbb{N}$:

$$E_x^{TE} = 0,$$
$$E_y^{TE} = -\mathcal{C}\frac{m\pi}{\mathtt{a}} \sin\left(\frac{m\pi z}{\mathtt{a}}\right) \cos\left(\frac{n\pi y}{\mathtt{b}}\right) e^{-\mathtt{i}\beta x},$$
$$E_z^{TE} = \mathcal{C}\frac{n\pi}{\mathtt{b}} \cos\left(\frac{m\pi z}{\mathtt{a}}\right) \sin\left(\frac{n\pi y}{\mathtt{b}}\right) e^{-\mathtt{i}\beta x}.$$

The real constant $\beta$ is linked to the waveguide dimensions $\mathtt{a}, \mathtt{b}$ by the so called dispersion relation $\left(\frac{m\pi}{\mathtt{a}}\right)^2 + \left(\frac{n\pi}{\mathtt{b}}\right)^2 = \tilde{\omega}^2 - \beta^2$, and we choose $\mathcal{C} = \mathtt{i}\omega\mu/(\tilde{\omega}^2 - \beta^2)$. The field $\mathbf{E}^{TE}$ satisfies the metallic boundary conditions on $\Gamma_{\text{w}}$ and the impedance boundary conditions on $\Gamma_{\text{in}}$, $\Gamma_{\text{out}}$ with parameter $\xi = \beta$ and $\mathbf{g}^{\text{in}} = (\mathtt{i}\beta + \mathtt{i}\beta)\mathbf{E}^{TE} = 2\mathtt{i}\beta\mathbf{E}^{TE}$ and $\mathbf{g}^{\text{out}} = (-\mathtt{i}\beta + \mathtt{i}\beta)\mathbf{E}^{TE} = \mathbf{0}$.

To cast the continuous problem (2.1) with metallic (resp. impedance) boundary conditions on $\Gamma_{\text{w}}$ (resp. $\Gamma_{\text{in}}$, $\Gamma_{\text{out}}$) in the weak form, one has to multiply (2.1) by a test function $\mathbf{v}$ of a suitable functional space $V$ and integrate by parts over the computational domain $\Omega$. More precisely, the weak problem reads: find $\mathbf{E} \in V$ such that

$$\int_\Omega \Big[(\nabla \times \mathbf{E}) \cdot (\nabla \times \mathbf{v}) - \gamma^2 \mathbf{E} \cdot \mathbf{v}\Big] + \int_{\Gamma_{\text{in}} \cup \Gamma_{\text{out}}} \mathtt{i}\xi (\mathbf{E} \times \mathbf{n}) \cdot (\mathbf{v} \times \mathbf{n})$$
$$= \int_{\Gamma_{\text{in}}} \mathbf{g}^{\text{in}} \cdot \mathbf{v} + \int_{\Gamma_{\text{out}}} \mathbf{g}^{\text{out}} \cdot \mathbf{v} \quad \forall \mathbf{v} \in V,$$

with $V = \{\mathbf{v} \in H(\text{curl}, \Omega), \mathbf{v} \times \mathbf{n} = 0 \text{ on } \Gamma_{\text{w}}\}$, where $H(\text{curl}, \Omega)$ is the space of square integrable functions whose curl is also square integrable. For a detailed discussion about existence and uniqueness of solutions we refer to [27].

**3. High order edge finite elements.** For a so-called compatible finite element (FE) discretization of the considered weak problem we need to introduce suitable discrete equivalents of the computational domain $\bar{\Omega}$ and of the functional space $H(\text{curl}, \Omega)$ where the mathematical unknown field lives. For the computational domain, complex interfaces where physical parameters, such as $\sigma$ or $\varepsilon$, can jump, are

simpler to accommodate if a simplicial (triangular in 2d, tetrahedral in 3d) mesh $\mathcal{T}_h$ is considered in $\bar{\Omega}$ ($h$ denotes the maximal diameter of simplices in $\mathcal{T}_h$). The unknown $\mathbf{E}$, together with the functional operators on it, have meaningful discrete equivalents if we work in the curl-conforming finite dimensional subspace $V_h \subset H(\mathrm{curl}, \Omega)$ of *Nédélec edge finite elements* [28]. For a simplex $T \in \mathcal{T}_h$, the local *lowest order basis functions* for the Nédélec curl-conforming space are associated with the oriented edges $e = \{n_i, n_j\}$ of $T$ as follows

$$\mathbf{w}^e = \lambda_{n_i} \nabla \lambda_{n_j} - \lambda_{n_j} \nabla \lambda_{n_i}, \tag{3.1}$$

where the $\lambda_{n_\ell}$ are the barycentric coordinates of a point $\mathbf{x} \in T$ with respect to the node $n_\ell$ of $T$ of Cartesian coordinates $\mathbf{x}_\ell$. The *degrees of freedom* (*dofs*) over $T$ are defined as the functionals

$$\xi_e \colon \mathbf{w} \mapsto \frac{1}{|e|} \int_e \mathbf{w} \cdot \mathbf{t}_e, \quad \forall\, e \in \mathcal{E}(T),$$

where $\mathbf{t}_e = \mathbf{x}_j - \mathbf{x}_i$ is the tangent vector to the edge $e$, $|e| = |\mathbf{t}_e|$ the length of $e$ and $\mathcal{E}(T)$ the set of edges of $T$. At the lowest order, the basis functions are in *duality* with the dofs, that is $\xi_e(\mathbf{w}^{e'}) = 1$, resp. 0, if $e = e'$, resp. if $e \neq e'$. As a consequence, the coefficients that define the Galerkin projection $\mathbf{E}_h$ of the field $\mathbf{E}$ onto $V_h$ are the *circulations* of $\mathbf{E}_h$ along the oriented edges $e$ of the simplicial mesh $\mathcal{T}_h$: locally, in each $T \in \mathcal{T}_h$, we have

$$\mathbf{E}(\mathbf{x}) \approx \mathbf{E}_h(\mathbf{x}) = \sum_{e \in \mathcal{E}(T)} c_e \mathbf{w}^e(\mathbf{x}), \quad \forall\, \mathbf{x} \in T, \qquad c_e = \frac{1}{|e|} \int_e \mathbf{E}_h \cdot \mathbf{t}_e.$$

In the lowest order case, the approximation error verifies $||\mathbf{E} - \mathbf{E}_h||_* = O(h)$, where $||.||_*$ is the $H(\mathrm{curl}, \Omega)$-norm. There are several reasons to rely on edge elements rather than on other FE discretizations of $H(\mathrm{curl}, \Omega)$ [5]. By construction, edge elements guarantee the continuity of the tangential components across inter-element interfaces, they thus fit the continuity properties of the electric field. This is also due to the close relationship between the edge element basis functions $\mathbf{w}^e$ and Whitney 1-forms [7], those differential forms that can be used to describe the electric field in a more geometrical mathematical formulation of Maxwell's equations. In addition, for propagation problems, edge elements are known to avoid the pollution of the numerical solution by spurious modes [6], [3].

High order curl-conforming finite elements of Nédélec type have become established techniques in computational electromagnetism. Their popularity for wave propagation problems is due to the fact that they are characterized by low numerical dispersion and dissipation errors. Moreover, at a fixed number of dofs, their numerical accuracy is higher.

**3.1. Local definition of high order edge elements.** We adopt here the high order generators of Nédélec elements presented in [29],[30]: the definition of these generators is rather simple since it only involves the barycentric coordinates of the simplex. To state the definition and further properties, we need to introduce multi-index notations. A multi-index is an array $\mathbf{k} = (k_1, \ldots, k_\nu)$ of $\nu$ integers $k_i \geq 0$, and its weight $k$ is $\sum_{i=1}^{\nu} k_i$. The set of multi-indices $\mathbf{k}$ with $\nu$ components and of weight $k$ is denoted $\mathcal{I}(\nu, k)$. If $d = 2, 3$ is the ambient space dimension, we consider $\nu \leq d+1$ and, given $\mathbf{k} \in \mathcal{I}(\nu, k)$, we set $\lambda^{\mathbf{k}} = \prod_{i=1}^{\nu} (\lambda_{n_i})^{k_i}$, where the $n_i$ are $\nu$ nodes of the

$d+1$ nodes of $T$. Now, in the generators definition we take $\nu = d+1$ and $k = r-1$, with $r$ the polynomial degree of the generators.

DEFINITION 3.1 (Generators). *The generators for Nédélec edge element spaces $W^1_{h,r}(T)$ of degree $r \geq 1$ in a simplex $T \in \mathcal{T}_h$ are the $\lambda^{\mathbf{k}}\mathbf{w}^e$, with $\mathbf{k} \in \mathcal{I}(d+1,k)$, $k = r-1$ and $e \in \mathcal{E}(T)$. The $\mathbf{w}^e$ are the low order edge basis functions* (3.1) *(notice that the polynomial degree of the $\mathbf{w}^e$ is $r = 1$ and they are obtained with $k = 0$).*

In Section 1.2 of [28] $W^1_{h,r}(T)$-unisolvent dofs are presented, for any $r \geq 1$ (the space $W^1_{h,r}(T)$ is indeed a discrete counterpart of $H(\mathrm{curl}, T)$). By relying on the generators introduced in Definition 3.1, the functionals in [28] can be recast in a new more friendly form as follows (see details in [4], which are inspired by [27]).

DEFINITION 3.2 (Degrees of freedom). *For $r \geq 1$, $d = 3$, the functionals*

$$\xi_e \colon \mathbf{w} \mapsto \frac{1}{|e|}\int_e (\mathbf{w}\cdot\mathbf{t}_e)\, q, \qquad \forall\, q \in \mathbb{P}_{r-1}(e),\ \forall\, e \in \mathcal{E}(T), \tag{3.2}$$

$$\xi_f \colon \mathbf{w} \mapsto \frac{1}{|f|}\int_f (\mathbf{w}\cdot\mathbf{t}_{f,i})\, q, \qquad \forall\, q \in \mathbb{P}_{r-2}(f),\ \forall\, f \in \mathcal{F}(T), \tag{3.3}$$

$$\mathbf{t}_{f,i} \text{ two independent sides of } f,\ i = 1,2,$$

$$\xi_T \colon \mathbf{w} \mapsto \frac{1}{|T|}\int_T (\mathbf{w}\cdot\mathbf{t}_{T,i})\, q, \qquad \forall\, q \in \mathbb{P}_{r-3}(T), \tag{3.4}$$

$$\mathbf{t}_{T,i} \text{ three independent sides of } T,\ i = 1,2,3,$$

*with $\mathcal{F}(T)$ the set of faces of $T$, are the dofs for a function $\mathbf{w} \in W^1_{h,r}(T)$. The norm of the vectors $\mathbf{t}_e, \mathbf{t}_{f,i}, \mathbf{t}_{T,i}$ is the length of the associated edge. We say that $e, f, T$ are the* supports *of the dofs $\xi_e, \xi_f, \xi_T$.*

Notice that for $d = 2$, the dofs are given only by (3.2) and (3.3) substituting $f$ with the triangle $T$; similarly, in the following, when $d = 2$, what concerns volumes should not be taken into account and what concerns faces $f$ actually concerns the triangle $T$.

REMARK 3.3. *To make it easier the computation of dofs, a convenient choice for the polynomials $q$ spanning the polynomial spaces over simplices $e, f, T$ that appear in Definition 3.2 is given by suitable products of the barycentric coordinates associated with the nodes of the considered simplex. The space $\mathbb{P}_\rho(S)$ of polynomials of degree $\leq \rho$ over a $p$-simplex $S$ (i.e. a simplex of dimension $1 \leq p \leq d$) can be generated by the products $\lambda^{\mathbf{k}} = \prod_{i=1}^{p+1} (\lambda_{n_i})^{k_i}$, with $\mathbf{k} \in \mathcal{I}(p+1,\rho)$ and $n_i$ being the nodes of $S$.*

The *classification* of dofs into edge-type, face-type, volume-type dofs can be done also for generators: volume-type generators contain (inside $\lambda^{\mathbf{k}}$ or $\mathbf{w}^e$) the barycentric coordinates w.r.t. all the nodes of a tetrahedron $T$, face-type generators contain the ones w.r.t. all and only the nodes of a face $f$, edge-type generators contain the ones w.r.t. only the nodes of an edge $e$. Notice that face-type (resp. volume-type) generators appear for $r > 1$ (resp. $r > 2$) (and the same happens for face-type and volume-type dofs). See the explicit list of generators for the case $d = 3, r = 2$ in Example 3.1. It turns out that dofs $\xi_e$ are 0 on face-type and volume-type generators, and dofs $\xi_f$ are 0 on volume-type generators.

For the high order case ($r > 1$), the fields $\lambda^{\mathbf{k}}\mathbf{w}^e$ in Definition 3.1 are generators for $W^1_{h,r}(T)$, but some of the face-type or volume-type generators are *linearly dependent*. The selection of generators that constitute an actual basis of $W^1_{h,r}(T)$ can be guided by the dofs in Definition 3.2. More precisely, as face-type (resp. volume-type) generators keep the ones associated with the two (resp. three) edges $e$ *chosen as* the two sides $\mathbf{t}_{f,1}, \mathbf{t}_{f,2}$ (resp. three sides $\mathbf{t}_{T,1}, \mathbf{t}_{T,2}, \mathbf{t}_{T,3}$) of face-type dofs (3.3) (resp. volume-type

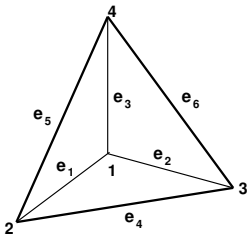


Fig. 3.1: For the tetrahedron in the figure, the edges are $e_1 = \{1,2\}$, $e_2 = \{1,3\}$, $e_3 = \{1,4\}$, $e_4 = \{2,3\}$, $e_5 = \{2,4\}$, $e_6 = \{3,4\}$, the faces are $f_1 = \{2,3,4\}$, $f_2 = \{1,3,4\}$, $f_3 = \{1,2,4\}$, $f_4 = \{1,2,3\}$ (notice that the face $f_i$ is the one opposite the node $i$).

dofs (3.4)). A convenient choice of sides is described in Subsection 3.2 and is the one adopted in Example 3.1. One can check that the total number of dofs $\xi_e, \xi_f, \xi_T$ in a simplex $T$ is equal to $\dim(W^1_{h,r}(T)) = (r+d)(r+d-1)\cdots(r+2)r/(d-1)!$.

The considered basis functions are not in *duality* with the dofs in Definition 3.2 when $r > 1$, namely, the matrix $V$ with entries the weights $V_{ij} = \xi_i(\mathbf{w}_j)$, $1 \le i,j \le \dim(W^1_{h,r}(T))$ after a suitable renumbering of dofs, is not the identity matrix for $r > 1$. Duality can be re-established, if necessary, by considering, as basis functions, *linear combinations* of the previous basis functions with coefficients given by the entries of $V^{-1}$ (see [4]). Notice that $V$ (and then $V^{-1}$) does not depend on the metric of the simplex $T$ for which its entries are calculated. Indeed, first of all notice that dofs in Definition 3.2 are conveniently normalized. Moreover, the $\xi_i(\mathbf{w}_j)$ are integrals of two addends of the type $\lambda^{\mathbf{k}'}\nabla\lambda_{n_i}\cdot\mathbf{t}_e$ (here $\lambda^{\mathbf{k}'}$ gathers the products of barycentric coordinates appearing in the basis functions and in $q$, and $\mathbf{t}_e$ stands also for $\mathbf{t}_{f,i}, \mathbf{t}_{T,i}$). Now, we have $\nabla\lambda_{n_i}\cdot\mathbf{t}_e = -1$ if $n_i$ is the first node of $e$, $+1$ if it is its second node, 0 if it isn't a node of $e$; so, in the end, only terms of the type $\lambda^{\mathbf{k}'}$ survive in the integral and the value of $\xi_i(\mathbf{w}_j)$ can be calculated using the 'magic formula' (it is a classical result, see for instance [29]): if $S$ is a $p$-simplex, $\frac{1}{|S|}\int_S \prod_{i=1}^{p+1}(\lambda_{n_i})^{k_i} = p!(\prod_{i=1}^{p+1} k_i!)/(p+\sum_{i=1}^{p+1} k_i)!$. This value is clearly independent of the metric of $T$. Moreover, the entries of $V^{-1}$ turn out to be *integer* numbers. See Example 3.1 for the case $d = 3, r = 2$.

Duality is needed for instance in FreeFem++, a free domain specific language (DSL) specialized for solving boundary value problems with variational methods [22]. Several FE spaces are available in FreeFem++, such as Nédélec edge elements of degree 1 of equation (3.1): after generating a tetrahedral mesh `Th`, a complex vector function `E` in that space is simply declared with the commands `fespace Vh(Th,Edge03d); Vh<complex> [Ex,Ey,Ez];`. The user can also add new finite elements, provided that the duality property is satisfied. For instance we implemented the edge elements in 3d of degree $2, 3$, which can be used, since FreeFem++ version 3.44, loading the plugin `load "Element_Mixte3d"` and substituting `Edge03d` with `Edge13d`, `Edge23d` respectively. A powerful tool of FreeFem++ is the interpolation of a function given by its analytical expression, or a function of a certain FE space, onto a desired FE space. It is this interpolation operator that requires duality.

EXAMPLE 3.1 ($d = 3$, $r = 2$). *If the edges and the faces of a tetrahedron are numbered as in Fig. 3.1, the basis functions are* $\mathbf{w}_j = \lambda_{\alpha_j}\mathbf{w}^{e_{\beta_j}}$, $1 \le j \le 20$,

*where the* 12 *edge-type basis functions have* $(\alpha_j)_{j=1}^{12} = (1,2,\ 1,3,\ 1,4,\ 2,3,\ 2,4,\ 3,4)$ *and* $(\beta_j)_{j=1}^{12} = (1,1,\ 2,2,\ 3,3,\ 4,4,\ 5,5,\ 6,6)$*, and the* 8 *face-type basis functions have* $(\alpha_j)_{j=13}^{20} = (4,3,\ 4,3,\ 4,2,\ 3,2)$ *and* $(\beta_j)_{j=13}^{20} = (4,5,\ 2,3,\ 1,3,\ 1,2)$*. In order to get a basis, i.e. a set of linearly independent generators, we have chosen to eliminate the (face-type) generators* $\mathbf{w}_{21} = \lambda_2 \mathbf{w}^{e_6}$*,* $\mathbf{w}_{22} = \lambda_1 \mathbf{w}^{e_6}$*,* $\mathbf{w}_{23} = \lambda_1 \mathbf{w}^{e_5}$*,* $\mathbf{w}_{24} = \lambda_1 \mathbf{w}^{e_4}$*. The corresponding edge-type dofs are:*

$$\xi_1 \colon \mathbf{w} \mapsto \frac{1}{|e_1|} \int_{e_1} (\mathbf{w} \cdot \mathbf{t}_{e_1})\, \lambda_1, \quad \xi_2 \colon \mathbf{w} \mapsto \frac{1}{|e_1|} \int_{e_1} (\mathbf{w} \cdot \mathbf{t}_{e_1})\, \lambda_2, \ \ldots$$
$$\xi_{11} \colon \mathbf{w} \mapsto \frac{1}{|e_6|} \int_{e_6} (\mathbf{w} \cdot \mathbf{t}_{e_6})\, \lambda_3, \quad \xi_{12} \colon \mathbf{w} \mapsto \frac{1}{|e_6|} \int_{e_6} (\mathbf{w} \cdot \mathbf{t}_{e_6})\, \lambda_4,$$

*and the face-type dofs are:*

$$\xi_{13} \colon \mathbf{w} \mapsto \frac{1}{|f_1|} \int_{f_1} (\mathbf{w} \cdot \mathbf{t}_{e_4}), \quad \xi_{14} \colon \mathbf{w} \mapsto \frac{1}{|f_1|} \int_{f_1} (\mathbf{w} \cdot \mathbf{t}_{e_5}), \ \ldots$$
$$\xi_{19} \colon \mathbf{w} \mapsto \frac{1}{|f_4|} \int_{f_4} (\mathbf{w} \cdot \mathbf{t}_{e_1}), \quad \xi_{20} \colon \mathbf{w} \mapsto \frac{1}{|f_4|} \int_{f_4} (\mathbf{w} \cdot \mathbf{t}_{e_2}).$$

*For this ordering and choice of generators and dofs, the 'dualizing' matrix* $V^{-1}$ *is*

$$V^{-1} = \begin{bmatrix}
4 & -2 & 0 & 0 & 0 & 0 & 0 & 0 & 0 & 0 & 0 & 0 & 0 & 0 & 0 & 0 & 0 & 0 & 0 & 0 \\
-2 & 4 & 0 & 0 & 0 & 0 & 0 & 0 & 0 & 0 & 0 & 0 & 0 & 0 & 0 & 0 & 0 & 0 & 0 & 0 \\
0 & 0 & 4 & -2 & 0 & 0 & 0 & 0 & 0 & 0 & 0 & 0 & 0 & 0 & 0 & 0 & 0 & 0 & 0 & 0 \\
0 & 0 & -2 & 4 & 0 & 0 & 0 & 0 & 0 & 0 & 0 & 0 & 0 & 0 & 0 & 0 & 0 & 0 & 0 & 0 \\
0 & 0 & 0 & 0 & 4 & -2 & 0 & 0 & 0 & 0 & 0 & 0 & 0 & 0 & 0 & 0 & 0 & 0 & 0 & 0 \\
0 & 0 & 0 & 0 & -2 & 4 & 0 & 0 & 0 & 0 & 0 & 0 & 0 & 0 & 0 & 0 & 0 & 0 & 0 & 0 \\
0 & 0 & 0 & 0 & 0 & 0 & 4 & -2 & 0 & 0 & 0 & 0 & 0 & 0 & 0 & 0 & 0 & 0 & 0 & 0 \\
0 & 0 & 0 & 0 & 0 & 0 & -2 & 4 & 0 & 0 & 0 & 0 & 0 & 0 & 0 & 0 & 0 & 0 & 0 & 0 \\
0 & 0 & 0 & 0 & 0 & 0 & 0 & 0 & 4 & -2 & 0 & 0 & 0 & 0 & 0 & 0 & 0 & 0 & 0 & 0 \\
0 & 0 & 0 & 0 & 0 & 0 & 0 & 0 & -2 & 4 & 0 & 0 & 0 & 0 & 0 & 0 & 0 & 0 & 0 & 0 \\
0 & 0 & 0 & 0 & 0 & 0 & 0 & 0 & 0 & 0 & 4 & -2 & 0 & 0 & 0 & 0 & 0 & 0 & 0 & 0 \\
0 & 0 & 0 & 0 & 0 & 0 & 0 & 0 & 0 & 0 & -2 & 4 & 0 & 0 & 0 & 0 & 0 & 0 & 0 & 0 \\
0 & 0 & 0 & 0 & 0 & 0 & -4 & -2 & 2 & -2 & 2 & 4 & 8 & -4 & 0 & 0 & 0 & 0 & 0 & 0 \\
0 & 0 & 0 & 0 & 0 & 0 & 2 & -2 & -4 & -2 & -4 & -2 & -4 & 8 & 0 & 0 & 0 & 0 & 0 & 0 \\
0 & 0 & -4 & -2 & 2 & -2 & 0 & 0 & 0 & 0 & 2 & 4 & 0 & 0 & 8 & -4 & 0 & 0 & 0 & 0 \\
0 & 0 & 2 & -2 & -4 & -2 & 0 & 0 & 0 & 0 & -4 & -2 & 0 & 0 & -4 & 8 & 0 & 0 & 0 & 0 \\
-4 & -2 & 0 & 0 & 2 & -2 & 0 & 0 & 2 & 4 & 0 & 0 & 0 & 0 & 0 & 0 & 8 & -4 & 0 & 0 \\
2 & -2 & 0 & 0 & -4 & -2 & 0 & 0 & -4 & -2 & 0 & 0 & 0 & 0 & 0 & 0 & -4 & 8 & 0 & 0 \\
-4 & -2 & 2 & -2 & 0 & 0 & 2 & 4 & 0 & 0 & 0 & 0 & 0 & 0 & 0 & 0 & 0 & 0 & 8 & -4 \\
2 & -2 & -4 & -2 & 0 & 0 & -4 & -2 & 0 & 0 & 0 & 0 & 0 & 0 & 0 & 0 & 0 & 0 & -4 & 8
\end{bmatrix}$$

**3.2. Implementation of the global construction.** The implementation of edge finite elements is quite delicate. Indeed, basis functions and dofs are associated with the *oriented* edges of mesh simplices: notice that the low order $\mathbf{w}^e$ and the high order $\lambda^{\mathbf{k}} \mathbf{w}^e$ generators change sign if the orientation of the edge $e$ is reversed. Moreover, recall that for $r > 1$, in order to get a set of linearly independent generators, we also have to *choose* 2 edges for each face $f$. Here we wish to construct basis functions *locally*, i.e. in each simplex of $\mathcal{T}_h$, in such a way that the contributions coming from simplices sharing edges or faces could be assembled properly inside the *global* matrix of the FE discretization. For this purpose, it is essential to orient in the *same* way edges shared by simplices and to choose the *same* 2 edges for faces shared by adjacent tetrahedra. We have this need also to construct dofs giving the coefficients for the interpolation operator if this latter required.

This need is satisfied using the *global numbers* of the mesh nodes (see Fig. 3.2). More precisely, to orient the edges $e$ of the basis functions and the vectors $\mathbf{t}_e, \mathbf{t}_{f,i}, i =$

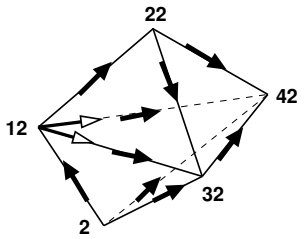


Fig. 3.2: Orientation of edges ('filled' arrows) and choice of 2 edges ('empty' arrows) of the face shared by two adjacent tetrahedra using the numbering of mesh nodes.

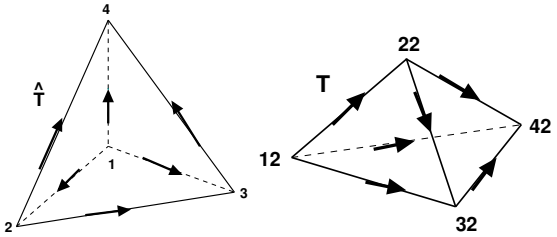


Fig. 3.3: Using global numbers to examine edges and faces, the 'structure of orientation' of $T = \{12, 32, 42, 22\}$ is the one of $\hat{T} = \{1, 2, 3, 4\}$ up to a rotation.

$1, 2, \mathbf{t}_{T,i}, i = 1, 2, 3$ of the dofs, we go from the node with the smallest global number to the node with the biggest global number. Similarly, to choose 2 edges per face for the face-type basis functions and dofs, we take the 2 edges going out from the node with the smallest global number in the face (and the 1st edge goes to the node with the 2nd smallest global number, the 2nd edge goes to the node with the biggest global number in the face).

Moreover, when we want basis functions $\tilde{\mathbf{w}}_j$ in duality with the dofs, a *second need* should be satisfied: we wish to use *for all mesh simplices* $T$ the 'dualizing' coefficients of the matrix $\hat{V}^{-1}$ calculated, once for all, for the reference simplex $\hat{T}$ *with* a certain choice of orientation and choice of edges (recall that $V^{-1}$ already does not depend on the metric of the simplex for which it is calculated). To be allowed to do this, it is sufficient to use the nodes *global numbers* to decide the order in which the non dual $\mathbf{w}_j$ (from which we start to then get the $\tilde{\mathbf{w}}_j$) are constructed locally on $T$. More precisely, for the edge-type (resp. face-type) basis functions the edges (resp. faces) are examined in the order written in the caption of Fig. 3.1, but replacing the nodes numbers $1, 2, 3, 4$ with the increasing global numbers of the nodes of $T$: the 1st examined edge is from the node with the 1st smallest global number to the one with the 2nd smallest global number, the 2nd examined edge is from the node with the 1st smallest global number to the one with the 3rd smallest global number, and so on, then the 1st examined face is the one opposite the node with the smallest global number, and so on. Indeed, in this way the first need is respected *and* the 'structure of orientation' of $T$ is the one of $\hat{T}$ up to a rotation (see Fig. 3.3): then we are allowed to use the coefficients of $\hat{V}^{-1}$ for the linear combinations giving the $\tilde{\mathbf{w}}_j$.

Notice that in 3d (resp. in 2d), to assemble the global linear system matrix, it is not essential which volume-type (resp. face-type) generators are chosen since they are

not shared between tetrahedra (resp. triangles). On the contrary, also this choice is important when we want to use for all mesh simplices the coefficients of $\hat{V}^{-1}$ calculated for a simplex with a certain choice of orientation and choice of edges.

EXAMPLE 3.2 (Implementation). *To implement the strategy described to construct locally the basis functions* $\tilde{\mathbf{w}}_j$*, two* permutations *can be used. First, to construct the non dual* $\mathbf{w}_j$*, we define a permutation* $p_{d+1}$ *of* $d+1$ *elements as follows:* $p_{d+1}[i]$ *is the local number (it takes values among* $1, \dots, d+1$*) of the node with the* $i$*-th smallest global number in the simplex* $T$*, so we can say that* $p_{d+1}$ *is the permutation for which the nodes of* $T$ *are listed with increasing global number. For instance, for the tetrahedron* $T = \{12, 32, 42, 22\}$ *in Fig. 3.3, we have* $p_4 = \{1, 4, 2, 3\}$*. So, in the first step of construction of the* $\mathbf{w}_j$*, we replace each* $\lambda_i$ *appearing in their expression with* $\lambda_{p_{d+1}[i]}$*. Then, in the second step of construction of the* $\tilde{\mathbf{w}}_j$ *as linear combinations of the* $\mathbf{w}_j$*, we use a permutation* $P_{n_{dofs}}$ *of* $n_{dofs} = \dim(W^1_{h,r}(T))$ *elements to go back to the local order of edges and faces. For instance for the tetrahedron* $T = \{12, 32, 42, 22\}$*, the order in which edges are examined in the first step is* $\{\{12, 22\}, \{12, 32\}, \{12, 42\}, \{22, 32\}, \{22, 42\}, \{32, 42\}\}$*, while the local order of edges would be* $\{\{12, 32\}, \{12, 42\}, \{12, 22\}, \{32, 42\}, \{22, 32\}, \{22, 42\}\}$ *(the local order is given by how the nodes of* $T$ *are listed); similarly, the order in which faces are examined in the first step is* $\{\{22, 32, 42\}, \{12, 32, 42\}, \{12, 22, 42\}, \{12, 22, 32\}\}$*, while the local order of faces would be* $\{\{22, 32, 42\}, \{12, 22, 42\}, \{12, 22, 32\}, \{12, 32, 42\}\}$*. So for this tetrahedron, if* $r = 2$ *(for which there are* 2 *basis functions for each edge and* 2 *basis functions for each face,* 20 *basis functions in total listed in Example 3.1), we have*

$$P_{20} = \{5, 6,\ 1, 2,\ 3, 4,\ 9, 10,\ 11, 12,\ 7, 8;\ 13, 14,\ 19, 20,\ 15, 16,\ 17, 18\},$$

*(notice that inside each edge or face the* 2 *related dofs remain ordered according to the global numbers). Now, we save the linear combinations of the* $\mathbf{w}_\ell$*, with coefficients given by the* $j$*-th column of* $\hat{V}^{-1}$*, in the final dual basis functions* $\tilde{\mathbf{w}}_{P_{20}[j]}$*.*

**4. Overlapping Schwarz preconditioners.** As shown numerically in [29], the matrix of the linear system resulting from the described high order discretization is ill conditioned. Therefore, we use and compare two domain decomposition preconditioners, *Restricted Additive Schwarz* (RAS) and *Additive Schwarz* (AS):

$$M^{-1}_{\mathrm{RAS}} = \sum_{s=1}^{N_{\mathrm{sub}}} \widetilde{R}_s^T A_s^{-1} R_s, \quad M^{-1}_{\mathrm{AS}} = \sum_{s=1}^{N_{\mathrm{sub}}} R_s^T A_s^{-1} R_s,$$

where $N_{\mathrm{sub}}$ is the number of overlapping subdomains $\Omega_s$ into which the domain $\Omega$ is decomposed. In this paper, the matrices $A_s$ are the local matrices of the *subproblems* with impedance boundary conditions $(\nabla \times \mathbf{E}) \times \mathbf{n} + \mathtt{i}\tilde{\omega}\mathbf{n} \times (\mathbf{E} \times \mathbf{n})$ as transmission conditions at the interfaces between subdomains. Notice that in this section the term 'local' refers to a subdomain and not to a mesh simplex.

In order to describe the matrices $R_s, \widetilde{R}_s$, let $\mathcal{N}$ be an ordered set of the degrees of freedom of the whole domain and let $\mathcal{N} = \bigcup_{s=1}^{N_{\mathrm{sub}}} \mathcal{N}_s$ be its decomposition into the (non disjoint) ordered subsets corresponding to the different (overlapping) subdomains $\Omega_s$: a degree of freedom belongs to $\mathcal{N}_s$ if its support is contained in $\Omega_s$. The matrix $R_s$ is the restriction matrix from $\Omega$ to the subdomain $\Omega_s$: it is a $\#\mathcal{N}_s \times \#\mathcal{N}$ Boolean matrix and its $(i, j)$ entry is equal to 1 if the $i$-th degree of freedom in $\mathcal{N}_s$ is the $j$-th one in $\mathcal{N}$. Notice that $R_s^T$ is then the extension matrix from the subdomain $\Omega_s$ to $\Omega$. The matrix $\widetilde{R}_s$ is a $\#\mathcal{N}_s \times \#\mathcal{N}$ restriction matrix like $R_s$, but with some of the unit

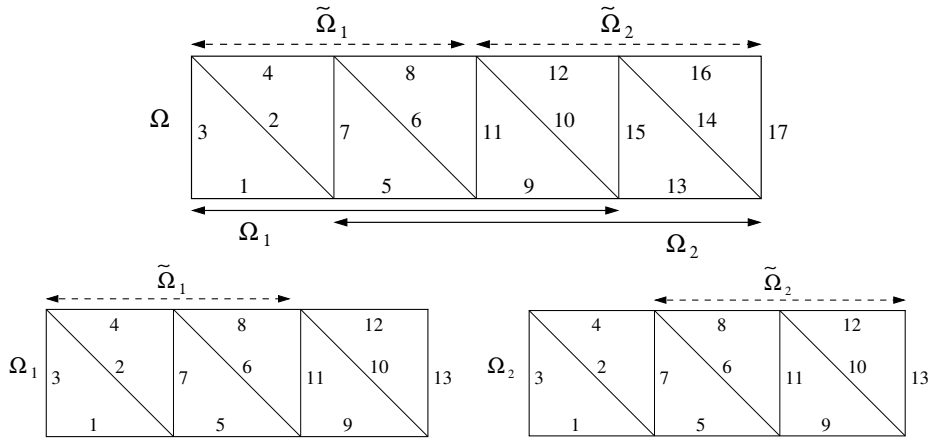


Fig. 4.1: Edges numbering for a domain $\Omega$ decomposed into two overlapping subdomains $\Omega_1$, $\Omega_2$ (above), and edges numbering for $\Omega_1$ and $\Omega_2$ (below). The non overlapping decomposition into $\widetilde{\Omega}_1$, $\widetilde{\Omega}_2$ is used to construct the matrices $\widetilde{R}_1$, $\widetilde{R}_2$.

entries corresponding to the overlap replaced by zeros: this would correspond to a decomposition into *non overlapping* subdomains $\widetilde{\Omega}_s \subset \Omega_s$ (completely non overlapping, not even on their border) (see [19]). This way $\sum_{s=1}^{N_{\text{sub}}} \widetilde{R}_s^T R_s = I$, that is the matrices $\widetilde{R}_s$ give a discrete partition of unity (which is made only of 1 and 0).

As an illustration, we write explicitly the restriction matrices $R_s, \widetilde{R}_s$ for the simple case shown in Fig. 4.1. The domain $\Omega$ is decomposed into two overlapping subdomains $\Omega_1, \Omega_2$, and edge finite elements of degree $r = 1$ are considered: the degrees of freedom are in correspondence with the edges of the mesh, so their order inside $\mathcal{N}$, $\mathcal{N}_1$, $\mathcal{N}_2$ is given by the edges numbering of the figure. Here, since $\#\mathcal{N}_1 = \#\mathcal{N}_2 = 13$, $\#\mathcal{N} = 17$, all restriction matrices have dimension $13 \times 17$. The matrices $\widetilde{R}_1$, $\widetilde{R}_2$ are constructed using the non overlapping subdomains $\widetilde{\Omega}_1$, $\widetilde{\Omega}_2$ shown in the figure (notice that the edge 11 of $\Omega$ is contained in $\widetilde{\Omega}_2$ and not in $\widetilde{\Omega}_1$). In the matrices below, if an entry is empty it should be equal to 0, and the bold zeros in $\widetilde{R}_1$, $\widetilde{R}_2$ are the zeros that replace unit entries in $R_1, R_2$:

$$R_1 = \begin{bmatrix} 1 & & & & & & & & & & & & \\ & 1 & & & & & & & & & & & \\ & & 1 & & & & & & & & & & \\ & & & 1 & & & & & & & & & \\ & & & & 1 & & & & & & & & \\ & & & & & 1 & & & & & & & \\ & & & & & & 1 & & & & & & \\ & & & & & & & 1 & & & & & \\ & & & & & & & & 1 & & & & \\ & & & & & & & & & 1 & & & \\ & & & & & & & & & & 1 & & \\ & & & & & & & & & & & 1 & \\ & & & & & & & & & & & & \mathbf{0\ 0\ 1\ 0\ 0} \end{bmatrix}, \quad R_2 = \begin{bmatrix} \mathbf{0\ 0\ 0\ 0\ 1} & & & & & & & & & & & & \\ & & & & & 1 & & & & & & & \\ & & & & & & 1 & & & & & & \\ & & & & & & & 1 & & & & & \\ & & & & & & & & 1 & & & & \\ & & & & & & & & & 1 & & & \\ & & & & & & & & & & 1 & & \\ & & & & & & & & & & & 1 & \\ & & & & & & & & & & & & 1 \\ & & & & & & & & & & & & \\ & & & & & & & & & & & & \\ & & & & & & & & & & & & \\ & & & & & & & & & & & & \end{bmatrix},$$

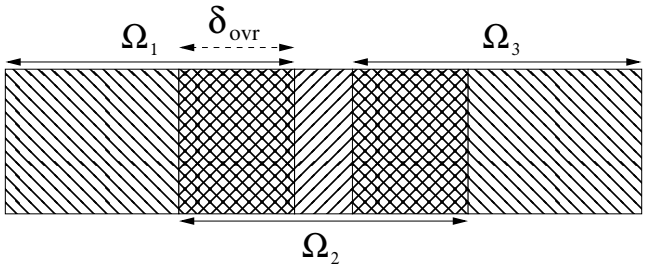


Fig. 4.2: The stripwise decomposition of the two-dimensional domain.

| $k$ | $N_{\text{dofs}}$ | $N_{\text{iterNp}}$ | $N_{\text{iter}}$ | $\max\lvert\lambda-(1,0)\rvert$ | $\#\{\lambda\in\mathbb{C}\setminus\bar{\mathcal{D}}_1\}$ | $\#\{\lambda\in\partial\mathcal{D}_1\}$ |
|---|---|---|---|---|---|---|
| 0 | 282 | 179 | 5(10) | $1.04e{-}1(1.38e{+}1)$ | 0(4) | 0(12) |
| 1 | 884 | 559 | 6(15) | $1.05e{-}1(1.63e{+}1)$ | 0(8) | 0(40) |
| 2 | 1806 | 1138 | 6(17) | $1.05e{-}1(1.96e{+}1)$ | 0(12) | 0(84) |
| 3 | 3048 | 1946 | 6(21) | $1.05e{-}1(8.36e{+}2)$ | 0(16) | 0(144) |
| 4 | 4610 | 2950 | 6(26) | $1.05e{-}1(1.57e{+}3)$ | 0(20) | 0(220) |

Table 4.1: Influence of the polynomial degree $r = k{+}1$ on the convergence of RAS(AS) preconditioner for $\omega = \omega_2$, $N_{\text{sub}} = 2$, $\delta_{\text{ovr}} = 2h$.

$$\widetilde{R}_1 = \begin{bmatrix} 1 & & & & & & & & & & & & & & \\ & 1 & & & & & & & & & & & & & \\ & & 1 & & & & & & & & & & & & \\ & & & 1 & & & & & & & & & & & \\ & & & & 1 & & & & & & & & & & \\ & & & & & 1 & & & & & & & & & \\ & & & & & & 1 & & & & & & & & \\ & & & & & & & 1 & & & & & & & \\ & & & & & & & & \mathbf{0} & & & & & & \\ & & & & & & & & & \mathbf{0} & & & & & \\ & & & & & & & & & & \mathbf{0} & & & & \\ & & & & & & & & & & & \mathbf{0} & & & \\ & & & & & & & & & & & & 0 & 0 & \mathbf{0} & 0 & 0 \end{bmatrix}, \quad \widetilde{R}_2 = \begin{bmatrix} 0 & 0 & 0 & 0 & \mathbf{0} & & & & & & & & & & \\ & & & & & \mathbf{0} & & & & & & & & & \\ & & & & & & \mathbf{0} & & & & & & & & \\ & & & & & & & \mathbf{0} & & & & & & & \\ & & & & & & & & 1 & & & & & & \\ & & & & & & & & & 1 & & & & & \\ & & & & & & & & & & 1 & & & & \\ & & & & & & & & & & & 1 & & & \\ & & & & & & & & & & & & 1 & & \\ & & & & & & & & & & & & & 1 & \\ & & & & & & & & & & & & & & 1 \end{bmatrix}.$$

**4.1. Numerical results.** We validate the preconditioners just described for a two-dimensional waveguide with $\mathtt{c} = 0.0502\,\text{m}$, $\mathtt{b} = 0.00254\,\text{m}$, with the physical parameters: $\varepsilon = 8.85 \cdot 10^{-12}\,\text{F}\,\text{m}^{-1}$, $\mu = 1.26 \cdot 10^{-6}\,\text{H}\,\text{m}^{-1}$ and $\sigma = 0.15\,\text{S}\,\text{m}^{-1}$. We consider three angular frequencies $\omega_1 = 16\,\text{GHz}$, $\omega_2 = 32\,\text{GHz}$, and $\omega_3 = 64\,\text{GHz}$, varying the mesh size $h$ according to the relation $h^2 \cdot \tilde{\omega}^3 = 2$ (in [25] it was proved that this relation avoids pollution effects for the one-dimensional Helmholtz equation).

We solve the linear system resulting from the finite element discretization with (MATLAB) GMRES (with a tolerance of $10^{-6}$), starting with a *random* initial guess, which ensures, unlike a zero initial guess, that all frequencies are present in the error. We compare the RAS and AS preconditioners, taking a stripwise subdomains decomposition, along the wave propagation, as shown in Fig. 4.2.

To study the convergence of GMRES preconditioned by RAS or AS we vary first the polynomial degree $r = k + 1$ (Table 4.1, Figs. 4.3–4.4, Fig. 4.12), then the angular frequency $\omega$ (Table 4.2, Figs. 4.5–4.6, Fig. 4.13), the number of subdomains

| $\omega$ | $N_{\text{dofs}}$ | $N_{\text{iterNp}}$ | $N_{\text{iter}}$ | $\max\lvert\lambda-(1,0)\rvert$ | $\#\{\lambda\in\mathbb{C}\setminus\bar{\mathcal{D}}_1\}$ | $\#\{\lambda\in\partial\mathcal{D}_1\}$ |
|---|---|---|---|---|---|---|
| $\omega_1$ | 339 | 232 | 5(11) | $2.46e{-}1(1.33e{+}1)$ | 0(6) | 0(45) |
| $\omega_2$ | 1806 | 1138 | 6(17) | $1.05e{-}1(1.96e{+}1)$ | 0(12) | 0(84) |
| $\omega_3$ | 7335 | 4068 | 9(24) | $3.03e{-}1(2.73e{+}1)$ | 0(18) | 0(123) |

Table 4.2: Influence of the angular frequency $\omega$ on the convergence of RAS(AS) preconditioner for $k=2$, $N_{\text{sub}}=2$, $\delta_{\text{ovr}}=2h$.

| $N_{\text{sub}}$ | $N_{\text{iter}}$ | $\max\lvert\lambda-(1,0)\rvert$ | $\#\{\lambda\in\mathbb{C}\setminus\bar{\mathcal{D}}_1\}$ | $\#\{\lambda\in\partial\mathcal{D}_1\}$ |
|---|---|---|---|---|
| 2 | 6(17) | $1.05e{-}1(1.96e{+}1)$ | 0(12) | 0(84) |
| 4 | 10(27) | $5.33e{-}1(1.96e{+}1)$ | 0(38) | 0(252) |
| 8 | 19(49) | $7.73e{-}1(1.96e{+}1)$ | 0(87) | 0(588) |

Table 4.3: Influence of the number of subdomains $N_{\text{sub}}$ on the convergence of RAS(AS) preconditioner for $k=2$, $\omega=\omega_2$, $\delta_{\text{ovr}}=2h$.

$N_{\text{sub}}$ (Table 4.3, Figs. 4.7–4.8, Fig. 4.14) and finally the overlap size $\delta_{\text{ovr}}$ (Table 4.4, Figs. 4.9–4.10, Fig. 4.15). Here, $\delta_{\text{ovr}}=1h,2h,4h$ means that we consider an overlap between two subdomains of $1,2,4$ mesh triangles along the horizontal direction.

In Tables 4.1–4.4, $N_{\text{dofs}}$ is the total number of degrees of freedom, $N_{\text{iterNp}}$ is the number of iterations necessary to attain the prescribed convergence for GMRES without any preconditioner, and $N_{\text{iter}}$ is the number of iterations for GMRES preconditioned by RAS (AS). Moreover, denoting by

$$\mathcal{D}_1=\{z\in\mathbb{C}:|z-z_0|<1\}$$

the unit disk centered at $z_0=(1,0)$ in the complex plane, we measure also the maximum distance to $(1,0)$ of the eigenvalues $\lambda$ of the preconditioned matrix, the number of eigenvalues that have distance greater than 1, and the number of eigenvalues that have distance equal to 1 (up to a tolerance of $10^{-10}$). This information is useful to characterize the convergence. Indeed, if $A$ is the matrix of the system to solve and $M^{-1}$ is the domain decomposition preconditioner, then $I-M^{-1}A$ is the iteration matrix of the domain decomposition method used as an iterative solver. So, a measure of the convergence of the domain decomposition solver would be to check whether the eigenvalues of the preconditioned matrix $M^{-1}A$ are contained in $\mathcal{D}_1$. When the domain decomposition method is used, like here, as a preconditioner, the distribution of the spectrum remains a good indicator of the convergence. Note that the matrix of the linear system doesn't change when $N_{\text{sub}}$ or $\delta_{\text{ovr}}$ vary, therefore in Tables 4.3–4.4 (where $k=2$, $\omega=\omega_2$) we don't report $N_{\text{dofs}}=1806$ and $N_{\text{iterNp}}=1155$ again. In all Tables 4.1–4.4, we don't mention the condition number of the preconditioned matrix: indeed, no convergence rate estimates in terms of the condition number of the matrix (which is not positive definite), as those we are used to with the conjugate gradient method, are available for the GMRES method.

Figs. 4.3, 4.5, 4.7, 4.9, respectively Figs. 4.4, 4.6, 4.8, 4.10, show the whole spectrum in the complex plane of the matrix preconditioned by RAS, respectively by AS (notice that many eigenvalues are multiple), together with $\partial\mathcal{D}_1$. Figs. 4.12–4.15 show

| $\delta_{\text{ovr}}$ | $N_{\text{iter}}$ | $\max\lvert\lambda-(1,0)\rvert$ | $\#\{\lambda\in\mathbb{C}\setminus\bar{\mathcal{D}}_1\}$ | $\#\{\lambda\in\partial\mathcal{D}_1\}$ |
|---|---|---|---|---|
| $1h$ | 10(20) | 1.95$e$+1(1.96$e$+1) | 3(12) | 0(39) |
| $2h$ | 6(17) | 1.05$e$−1(1.96$e$+1) | 0(12) | 0(84) |
| $4h$ | 5(14) | 1.06$e$−1(1.96$e$+1) | 0(12) | 0(174) |

Table 4.4: Influence of the overlap size $\delta_{\text{ovr}}$ on the convergence of RAS(AS) preconditioner for $k=2$, $\omega=\omega_2$, $N_{\text{sub}}=2$.

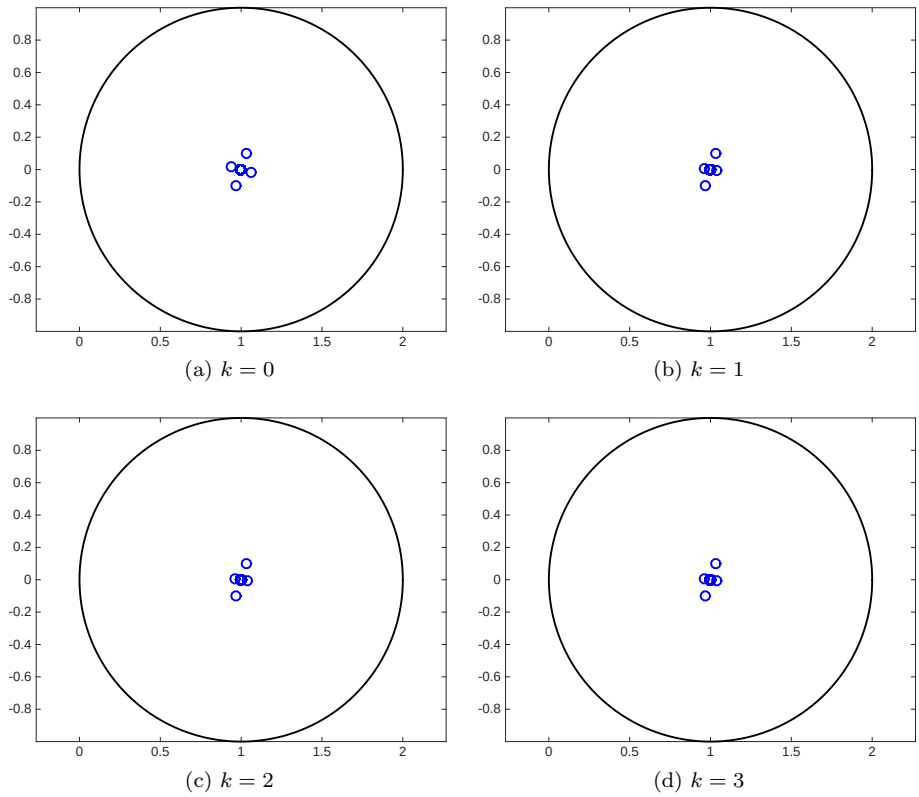

(a) $k=0$ (b) $k=1$

(c) $k=2$ (d) $k=3$

Fig. 4.3: Influence of the polynomial degree $r=k+1$ on the spectrum of the RAS-preconditioned matrix for $\omega=\omega_2$, $N_{\text{sub}}=2$, $\delta_{\text{ovr}}=2h$.

the evolution of the relative residual during the iterations of GMRES preconditioned with RAS (left) and AS (right).

Looking at the tables and figures, we can see that the non preconditioned GMRES method is very slow, and the RAS preconditioner gives much faster convergence than the AS preconditioner. Moreover, the convergence becomes slower when $k$, $\omega$ or $N_{\text{sub}}$ increase, or when $\delta_{\text{ovr}}$ decreases; actually, when varying $k$, the number of iterations for convergence using the RAS preconditioner is equal to 5 for $k=0$ and then it stays equal to 6 for $k>0$.

Notice also that for 2 subdomains the spectrum is well clustered inside the unit disk when using the RAS preconditioner, except for the case with $\delta_{\text{ovr}}=1h$ (see

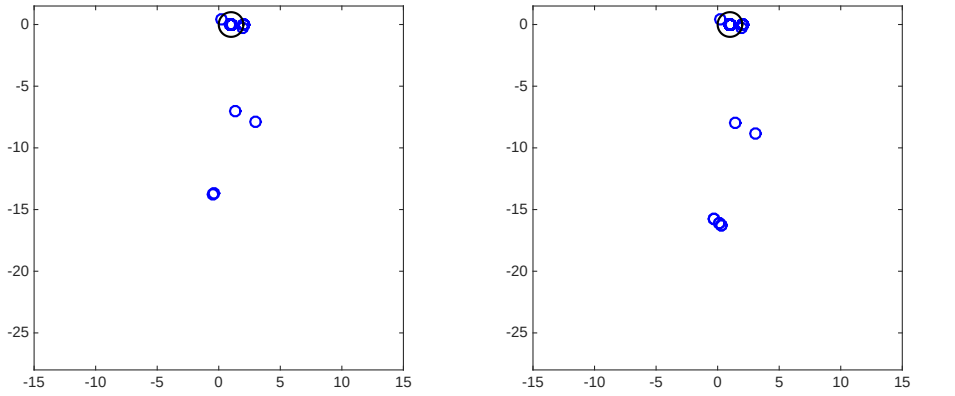


(a) $k = 0$




(b) $k = 1$

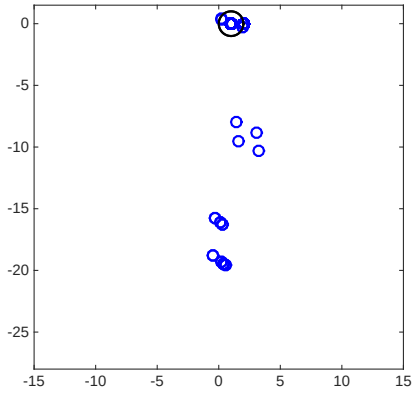


(c) $k = 2$

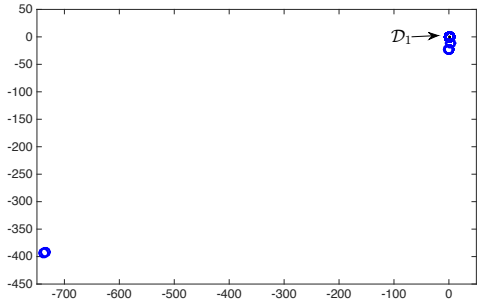


(d) $k = 3$

Fig. 4.4: Influence of the polynomial degree $r = k + 1$ on the spectrum of the AS-preconditioned matrix for $\omega = \omega_2$, $N_{\text{sub}} = 2$, $\delta_{\text{ovr}} = 2h$.

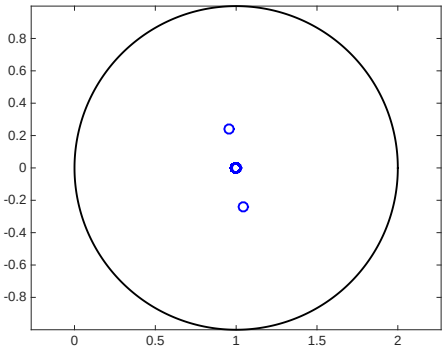


(a) $\omega = \omega_1$

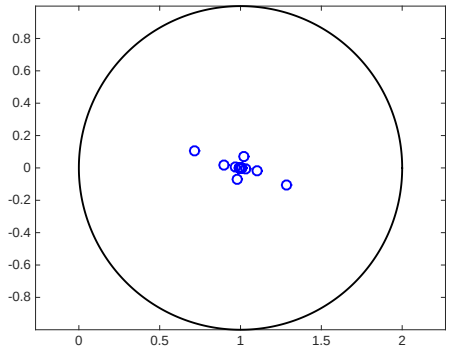


(b) $\omega = \omega_3$

Fig. 4.5: Influence of the angular frequency $\omega$ on the spectrum of the RAS-preconditioned matrix for $k = 2$, $N_{\text{sub}} = 2$, $\delta_{\text{ovr}} = 2h$.

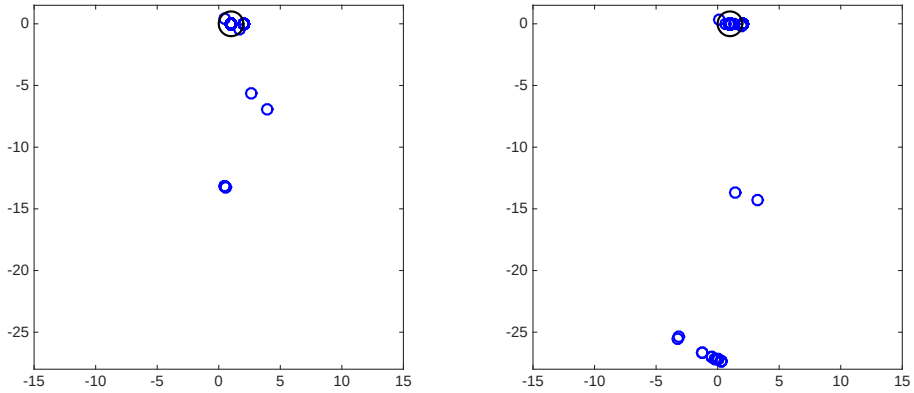

(a) $\omega = \omega_1$ (b) $\omega = \omega_3$

Fig. 4.6: Influence of the angular frequency $\omega$ on the spectrum of the AS-preconditioned matrix for $k = 2$, $N_{\text{sub}} = 2$, $\delta_{\text{ovr}} = 2h$.

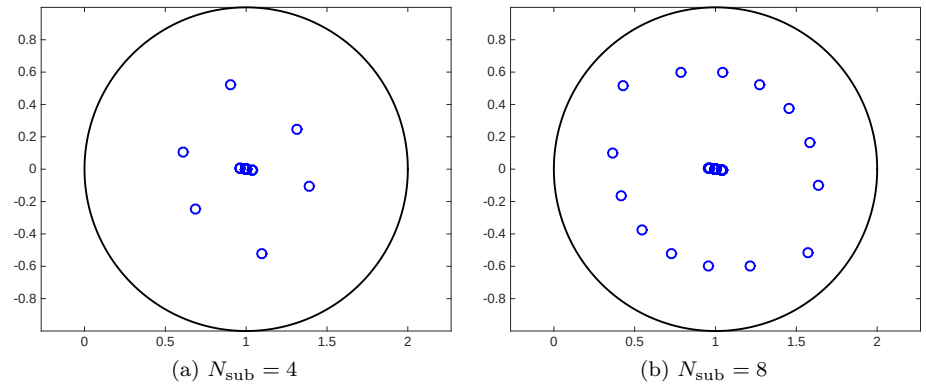

(a) $N_{\text{sub}} = 4$ (b) $N_{\text{sub}} = 8$

Fig. 4.7: Influence of the number of subdomains $N_{\text{sub}}$ on the spectrum of the RAS-preconditioned matrix for $k = 2$, $\omega = \omega_2$, $\delta_{\text{ovr}} = 2h$.

Fig. 4.11), in which 3 eigenvalues are outside with distances from $(1, 0)$ equal to $19.5, 19.4, 14.4$. Then, for 4 and 8 subdomains the spectrum is not so well clustered. With the AS preconditioner there are always eigenvalues outside the unit disk. For all the considered cases, the less clustered the spectrum, the slower the convergence.

**5. A three-dimensional example.** We complete the presentation showing some results for the 3d case. Again the physical parameters are: $\varepsilon = 8.85{\cdot}10^{-12}\,\mathrm{F\,m^{-1}}$, $\mu = 1.26{\cdot}10^{-6}\,\mathrm{H\,m^{-1}}$ and $\sigma = 0.15\,\mathrm{S\,m^{-1}}$; the waveguide dimensions are $\mathtt{c} = 0.0502\,\mathrm{m}$, $\mathtt{b} = 0.00254\,\mathrm{m}$, and $\mathtt{a} = 0.00508\,\mathrm{m}$ and we take a stripwise subdomains decomposition along the wave propagation, with $\delta_{\text{ovr}} = 2h$. Since the propagation constant in 3d is $\beta$ (see Section 2) and no more $\tilde{\omega}$, we compute the mesh size $h$ using the relation $h^2 \cdot \beta^3 = 1$, taking $\beta = \omega_\beta \sqrt{\mu\varepsilon}$, with $\omega_\beta = 32\,\mathrm{GHz}$. Then the dispersion relation gives $\tilde{\omega} = \sqrt{\beta^2 + (m\pi/\mathtt{a})^2 + (n\pi/\mathtt{b})^2}$ (where we choose $m = 1, n = 0$), and we get $\omega = \tilde{\omega}/\sqrt{\mu\varepsilon}$.

Here, the global linear system matrix and right-hand side, and all the matrices

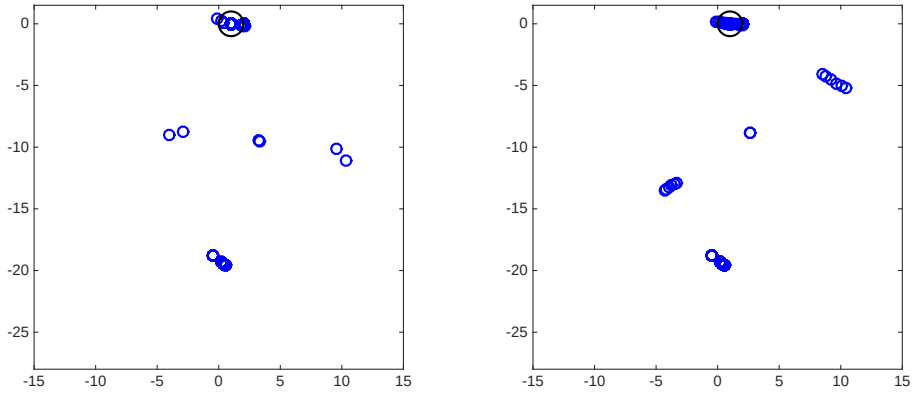


(a) $N_{\text{sub}} = 4$ (b) $N_{\text{sub}} = 8$

Fig. 4.8: Influence of the number of subdomains $N_{\text{sub}}$ on the spectrum of the AS-preconditioned matrix for $k = 2$, $\omega = \omega_2$, $\delta_{\text{ovr}} = 2h$.

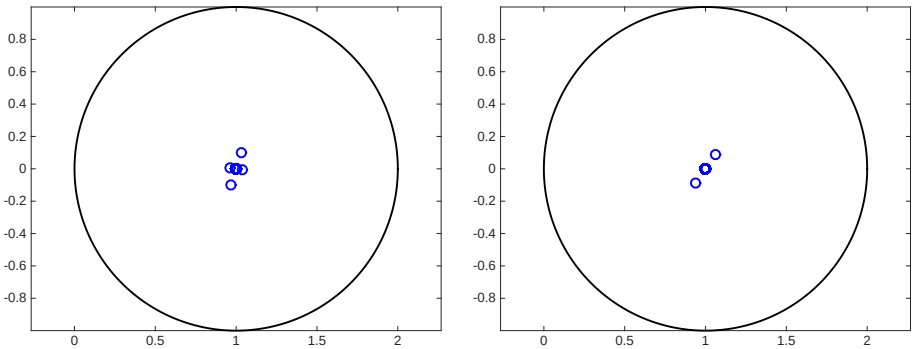


(a) $\delta_{\text{ovr}} = 2h$ (b) $\delta_{\text{ovr}} = 4h$

Fig. 4.9: Influence of the overlap size $\delta_{\text{ovr}}$ on the spectrum of the RAS-preconditioned matrix for $k = 2$, $\omega = \omega_2$, $N_{\text{sub}} = 2$.

appearing in RAS and AS preconditioners are built in a FreeFem++ script, and the form of RAS preconditioner is slightly different:

$$M_{\text{RAS}}^{-1} = \sum_{s=1}^{N_{\text{sub}}} R_s^T D_s A_s^{-1} R_s,$$

where the $\#\mathcal{N}_s \times \#\mathcal{N}_s$ diagonal matrices $D_s$ give the discrete partition of unity (here they may contain entries different from 1 and 0). The implementation of this partition of unity is inspired by the one of HPDDM [26], a high-performance unified framework for domain decomposition methods which is interfaced with FreeFem++; the partition of unity is then adapted for high order edge elements. Like in the 2d case, the linear system is then solved with the preconditioned MATLAB GMRES, with a tolerance of $10^{-6}$ and starting with a random initial guess.

In Table 5.1 we show the number of iterations for convergence varying first the polynomial degree $r = k+1$ (for $N_{\text{sub}} = 2$), and then the number of subdomains $N_{\text{sub}}$

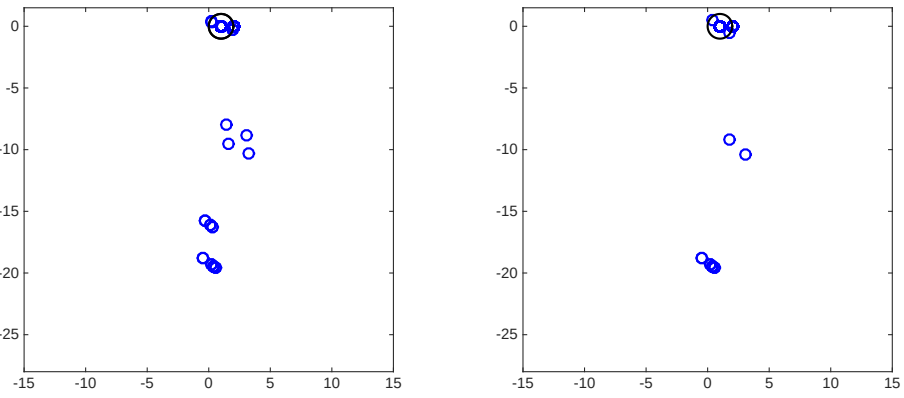

(a) $\delta_{\text{ovr}} = 2h$ (b) $\delta_{\text{ovr}} = 4h$

Fig. 4.10: Influence of the overlap size $\delta_{\text{ovr}}$ on the spectrum of the AS-preconditioned matrix for $k = 2$, $\omega = \omega_2$, $N_{\text{sub}} = 2$.

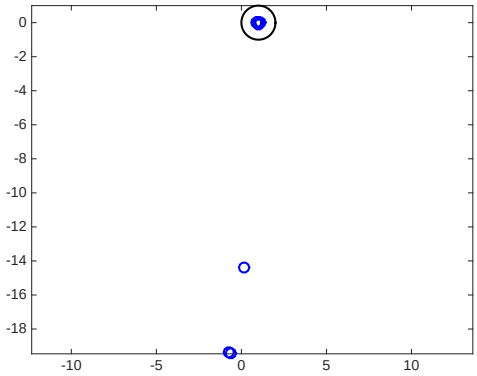

Fig. 4.11: The spectrum of the RAS-preconditioned matrix for $k = 2$, $\omega = \omega_2$, $N_{\text{sub}} = 2$, $\delta_{\text{ovr}} = 1h$.

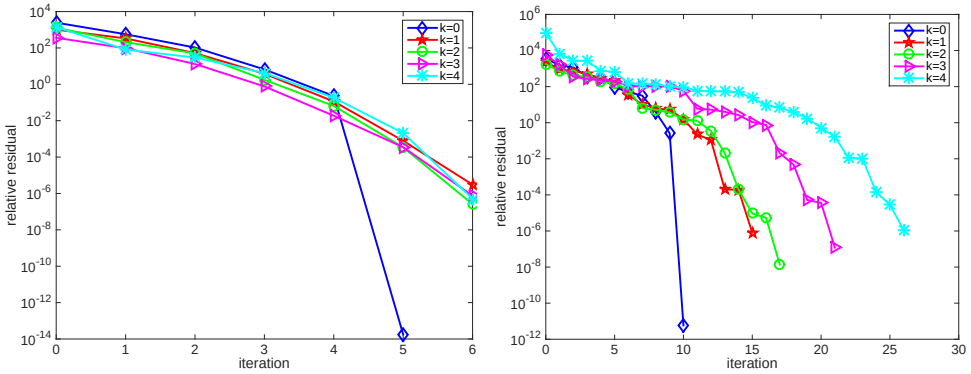


Fig. 4.12: Convergence history of GMRES preconditioned with RAS (left) and AS (right), for different polynomial degrees $r = k + 1$ ($\omega = \omega_2$, $N_{\text{sub}} = 2$, $\delta_{\text{ovr}} = 2h$).

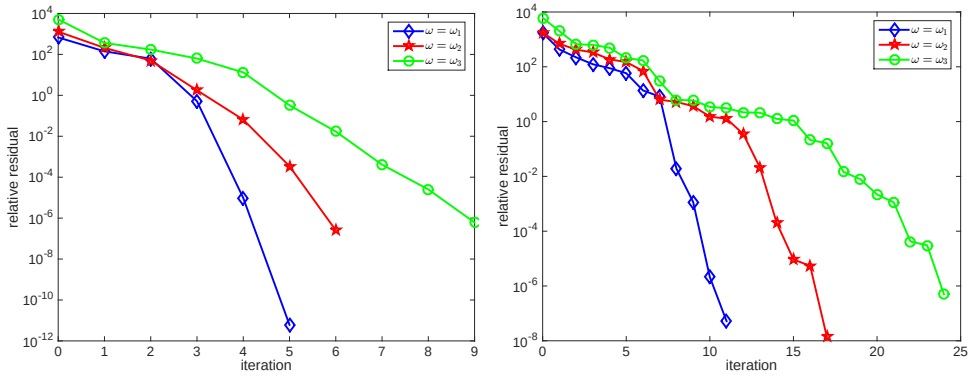


Fig. 4.13: Convergence history of GMRES preconditioned with RAS (left) and AS (right), for different angular frequencies $\omega$ ($k = 2$, $N_{\text{sub}} = 2$, $\delta_{\text{ovr}} = 2h$).

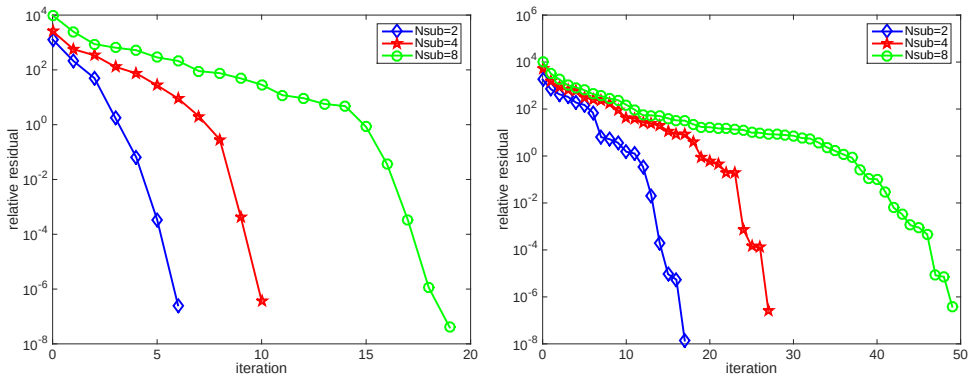


Fig. 4.14: Convergence history of GMRES preconditioned with RAS (left) and AS (right), for different numbers of subdomains $N_{\text{sub}}$ ($k = 2$, $\omega = \omega_2$, $\delta_{\text{ovr}} = 2h$).

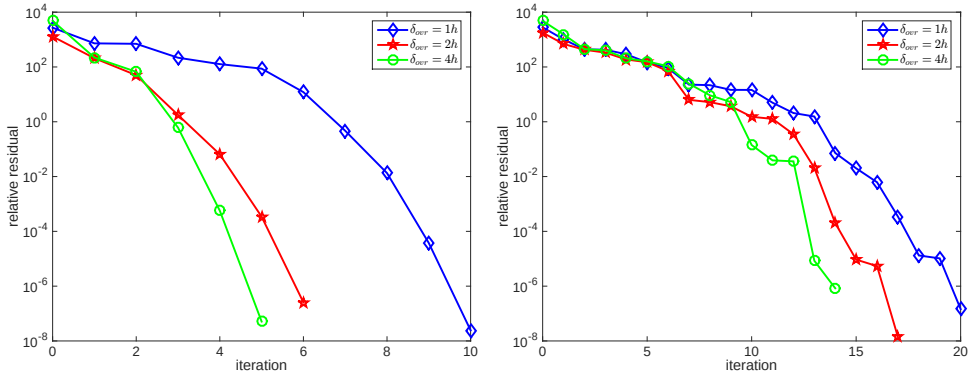


Fig. 4.15: Convergence history of GMRES preconditioned with RAS (left) and AS (right), for different overlap sizes $\delta_{\text{ovr}}$ ($k = 2$, $\omega = \omega_2$, $N_{\text{sub}} = 2$).

| $k$ | $N_{\text{dofs}}$ | $N_{\text{iter}}$ | $N_{\text{sub}}$ | $N_{\text{dofs}}$ | $N_{\text{iter}}$ |
|---|---|---|---|---|---|
| 0 | 8687 | 8(30) | 2 | 43654 | 9(55) |
| 1 | 43654 | 9(55) | 4 | 43654 | 12(70) |
| 2 | 123045 | 9(78) | 8 | 43654 | 20(100) |

Table 5.1: Results in 3d: influence of the polynomial degree $r = k + 1$ (for $N_{\text{sub}} = 2$), and of the number of subdomains $N_{\text{sub}}$ (for $k = 1$), on the convergence of RAS(AS) preconditioner ($\beta = \omega_\beta \sqrt{\mu\varepsilon}$ with $\omega_\beta = 32\,\text{GHz}$, $\delta_{\text{ovr}} = 2h$).

(for $k = 1$). Like in the 2d case, the number of iterations using the RAS preconditioner does not vary with the polynomial degree of the FE basis functions, while using the AS preconditioner it varies and is much higher. Again, the convergence becomes slower when the number of subdomains increases, both with RAS and AS.

In Figure 5.1 we plot the amplitude of the real part of the solution, which decreases as the wave propagates since $\sigma = 0.15\,\text{S}\,\text{m}^{-1}$ is different from zero.

**6. Conclusion.** We have adopted a friendly definition of high order edge elements generators and degrees of freedom: both in 2d and 3d their expression is rather simple, and the generators are strictly connected with the degrees of freedom. Their presentation is enriched with illustrative examples, and an operational strategy of implementation of these elements is described in detail. The elements in 3d of polynomial degree $1, 2, 3$ are available in FreeFem++ (since version 3.44), loading the plugin `load "Element_Mixte3d"` and building the finite element space `fespace` with the keywords `Edge03d`, `Edge13d`, `Edge23d` respectively.

Numerical experiments have shown that Schwarz preconditioning significantly improves GMRES convergence for different values of physical and numerical parameters, and that the RAS preconditioner always performs much better than the AS preconditioner. Indeed, the only advantage of the AS method is to preserve symmetry for symmetric problems: that is why it should be used only for symmetric positive definite matrices as a preconditioner for the conjugate gradient method. Moreover, in all the considered test cases, the number of iterations for convergence using the RAS preconditioner does not vary when the polynomial degree of the adopted high order finite elements increases.

However the computational cost per iteration grows since matrices become very large, therefore a parallel implementation should be considered. A two-level preconditioner via a coarse space correction should be designed for Maxwell's equations in order to fix the dependence on the number of subdomains of the iteration count.

REFERENCES

[1] M. Ainsworth and J. Coyle. Hierarchic finite element bases on unstructured tetrahedral meshes. *Internat. J. Numer. Methods Engrg.*, 58(14):2103–2130, 2003.

[2] D. N. Arnold, R. S. Falk, and R. Winther. Finite element exterior calculus, homological techniques, and applications. *Acta Numer.*, 15:1–155, 2006.

[3] D. Boffi, P. Fernandes, L. Gastaldi, and I. Perugia. Computational models of electromagnetic resonators: analysis of edge element approximation. *SIAM J. Numer. Anal.*, 36(4):1264–1290, 1999.

[4] M. Bonazzoli and F. Rapetti. High order finite elements in numerical electromagnetism: degrees of freedom and generators in duality. *preprint*, 2015.

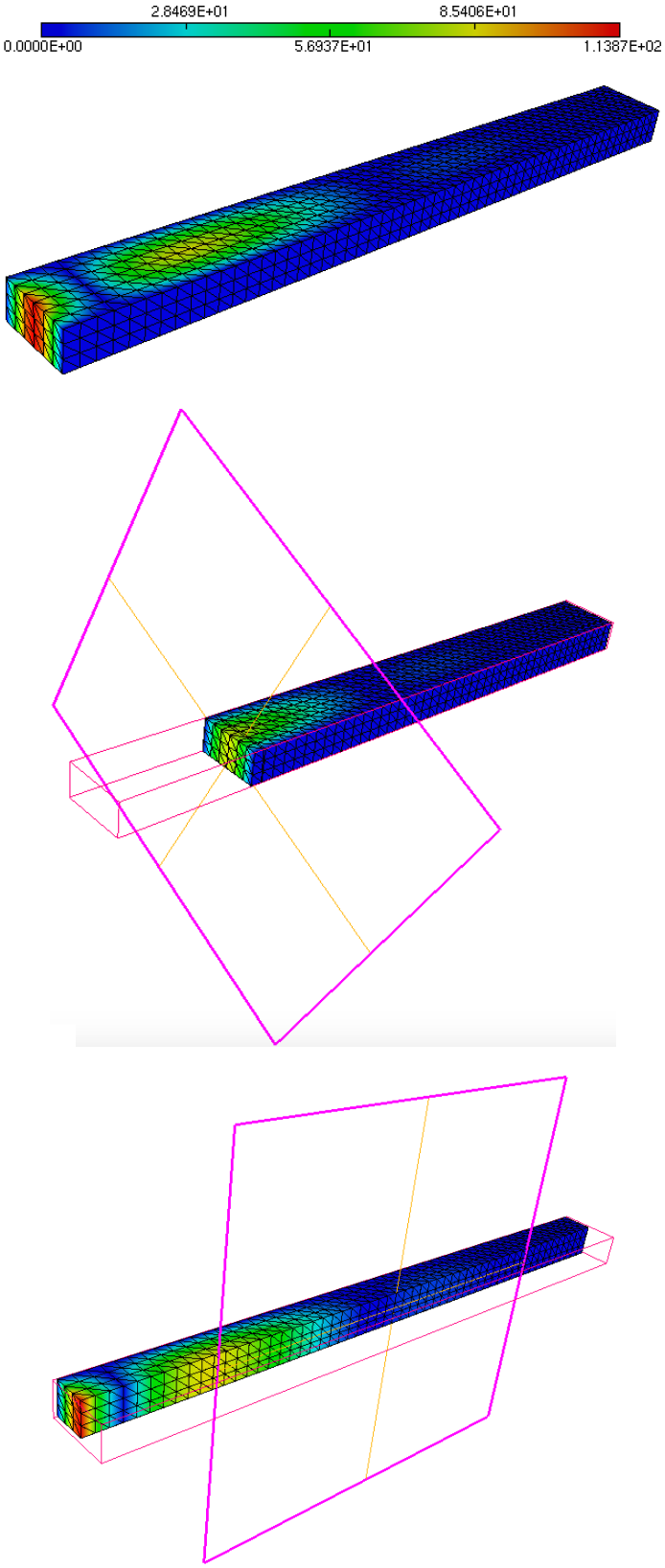


Fig. 5.1: The amplitude of the real part of the solution for $\sigma = 0.15\,\mathrm{S\,m^{-1}}$, with two sections of the waveguide.

[5] A. Bossavit. A rationale for 'edge-elements' in 3-d fields computations. *Magnetics, IEEE Transactions on*, 24(1):74–79, Jan 1988.
[6] A. Bossavit. Solving Maxwell equations in a closed cavity, and the question of 'spurious modes'. *Magnetics, IEEE Transactions on*, 26(2):702–705, Mar 1990.
[7] A. Bossavit. *Computational electromagnetism*. Electromagnetism. Academic Press, Inc., San Diego, CA, 1998. Variational formulations, complementarity, edge elements.
[8] P. Collino, G. Delbue, P. Joly, and A. Piacentini. A new interface condition in the non-overlapping domain decomposition for the Maxwell equations Helmholtz equation and related optimal control. *Comput. Methods Appl. Mech. Engrg*, 148:195–207, 1997.
[9] B. Després, P. Joly, and J. E. Roberts. A domain decomposition method for the harmonic Maxwell equations. In *Iterative methods in linear algebra (Brussels, 1991)*, pages 475–484, Amsterdam, 1992. North-Holland.
[10] V. Dolean, M. J. Gander, and L. Gerardo-Giorda. Optimized Schwarz methods for Maxwell's equations. *SIAM J. Sci. Comput.*, 31(3):2193–2213, 2009.
[11] V. Dolean, M. J. Gander, S. Lanteri, J.-F. Lee, and Z. Peng. Optimized Schwarz methods for curl-curl time-harmonic Maxwell's equations. In Jocelyne Erhel, Martin J. Gander, Laurence Halpern, Taoufik Sassi, and Olof Widlund, editors, *Proceedings of the 21st international domain decomposition conference*. Springer LNCSE, 2013.
[12] V. Dolean, M. J. Gander, S. Lanteri, J.-F. Lee, and Z. Peng. Effective transmission conditions for domain decomposition methods applied to the time-harmonic curl-curl Maxwell's equations. *J. Comput. Phys.*, 280:232–247, 2015.
[13] V. Dolean, L. Gerardo-Giorda, and M. J. Gander. Optimized Schwarz methods for Maxwell equations. *SIAM J. Scient. Comp.*, 31(3):2193–2213, 2009.
[14] V. Dolean, P. Jolivet, and F. Nataf. *An Introduction to Domain Decomposition Methods: algorithms, theory and parallel implementation*. SIAM, 2015.
[15] V. Dolean, S. Lanteri, and R. Perrussel. A domain decomposition method for solving the three-dimensional time-harmonic Maxwell equations discretized by discontinuous Galerkin methods. *J. Comput. Phys.*, 227(3):2044–2072, 2008.
[16] V. Dolean, S. Lanteri, and R. Perrussel. Optimized Schwarz algorithms for solving time-harmonic Maxwell's equations discretized by a discontinuous Galerkin method. *IEEE. Trans. Magn.*, 44(6):954–957, 2008.
[17] M. El Bouajaji, V. Dolean, M. J. Gander, and S. Lanteri. Optimized Schwarz methods for the time-harmonic Maxwell equations with dampimg. *SIAM J. Scient. Comp.*, 34(4):2048–2071, 2012.
[18] O. G. Ernst and M. J. Gander. Why it is difficult to solve Helmholtz problems with classical iterative methods. In *Numerical analysis of multiscale problems*, volume 83 of *Lect. Notes Comput. Sci. Eng.*, pages 325–363. Springer, Heidelberg, 2012.
[19] M. J. Gander. Schwarz methods over the course of time. *Electron. Trans. Numer. Anal.*, 31:228–255, 2008.
[20] M. J. Gander, F. Magoulès, and F. Nataf. Optimized Schwarz methods without overlap for the Helmholtz equation. *SIAM J. Sci. Comput.*, 24(1):38–60, 2002.
[21] J. Gopalakrishnan, L. E. García-Castillo, and L. F. Demkowicz. Nédélec spaces in affine coordinates. *Comput. Math. Appl.*, 49(7-8):1285–1294, 2005.
[22] F. Hecht. New development in FreeFem++. *J. Numer. Math.*, 20(3-4):251–265, 2012.
[23] R. Hiptmair. Canonical construction of finite elements. *Math. Comp.*, 68(228):1325–1346, 1999.
[24] R. Hiptmair. Finite elements in computational electromagnetism. *Acta Numer.*, 11:237–339, 2002.
[25] F. Ihlenburg and I. Babuška. Finite element solution of the Helmholtz equation with high wave number. I. The $h$-version of the FEM. *Comput. Math. Appl.*, 30(9):9–37, 1995.
[26] P. Jolivet, F. Hecht, F. Nataf, and C. Prud'Homme. Scalable domain decomposition preconditioners for heterogeneous elliptic problems. In *Proc. of the Int. Conference on High Performance Computing, Networking, Storage and Analysis*, pages 1–11. IEEE, 2013.
[27] P. Monk. *Finite element methods for Maxwell's equations*. Numerical Mathematics and Scientific Computation. Oxford University Press, New York, 2003.
[28] J.-C. Nédélec. Mixed finite elements in $\mathbf{R}^3$. *Numer. Math.*, 35(3):315–341, 1980.
[29] F. Rapetti. High order edge elements on simplicial meshes. *M2AN Math. Model. Numer. Anal.*, 41(6):1001–1020, 2007.
[30] F. Rapetti and A. Bossavit. Whitney forms of higher degree. *SIAM J. Numer. Anal.*, 47(3):2369–2386, 2009.
[31] J. Schöberl and S. Zaglmayr. High order Nédélec elements with local complete sequence properties. *COMPEL*, 24(2):374–384, 2005.